Sonochemical Route for Self-Assembled V_2O_5 Bundles with Spindle-like Morphology and Their Novel Application in Serum Albumin Sensing

Chang-Jie Mao, Hong-Cheng Pan, Xing-Cai Wu, Jun-Jie Zhu,* and Hong-Yuan Chen

Key Lab of Analytical Chemistry for Life Science, School of Chemistry and Chemical Engineering, Nanjing University, Nanjing 210093, P.R. China

Received: March 23, 2006; In Final Form: June 4, 2006

Novel self-assembled V_2O_5 bundles with highly ordered superstructures and spindle-like morphology were synthesized by a rapid high-yielding sonochemical method. The as-prepared samples were characterized by X-ray diffraction, a field-emission scanning electron microscope, and a transmission electron microscope. The spindle-like V_2O_5 bundles are composed of several tens of homogeneous nanowires with diameters of 30−50 nm and lengths of 3−7 μm. A sensitive resonance light scattering method for the detection of bovine serum albumin (BSA) based on the self-assembled V_2O_5 bundles was developed. The results of the polarized resonance light scattering demonstrated that the Cabannes factor for the V_2O_5 bundles−BSA aggregates was BSA concentration-dependent.

Introduction

Vanadium oxide (V_2O_5) nanostructures have attracted considerable attention because of their interesting layered structure, permitting a wide variety of molecules or cations to be embedded between the layers, which render them useful for gas-sensing applications. Generally, gas sensors fabricated by nanostructured V_2O_5 are based on a conductivity mechanism in which surface charge electron-depletion is strongly associated with the ionic character of the O−H bonds.[1−3] If vanadium oxides are in contact with some gases, the surface conductance changes, thus indicating the presence of the gas.[4] Due to specific morphology and a high volume−surface ratio, one-dimensional (1D) V_2O_5 nanostructures hold great promise as ethanol-sensing materials. The research group of Livage and Backov reported the preparation of macroscopic V_2O_5 fibers with a strong intrinsic 1D organization of V_2O_5 nanoscopic ribbon subunits.[1] These fibers demonstrated good selectivity as well as a strong and fast sensitivity in sensing alcohol vapor, with a detection limit of 0.1 ppm ethanol detected within 16 s at 40 °C. The Li group reported the development of highly selective and stable ethanol sensors based on single-crystalline vanadium oxide nanobelts.[3] The gas sensors have been shown to have great potential for the detection of ethanol molecules at a relatively low temperature.

Although there are several approaches to the synthesis of 1D nanostructured V_2O_5,[5−10] the organization of 1D V_2O_5 nanostructured subunits into highly ordered superstructures still remains a challenge. Making use of an extrusion process, the research group of Livage and Backov fabricated macroscopic V_2O_5 fibers which are constituted of nanoscopic ribbon subunits with strong preferential orientation parallel to the main axis of the fibers.[1] Wan and co-workers developed a mediated polyol process to synthesize V_2O_5 with highly ordered superstructures in which nanoparticles interconnect to form nanorods, and these rods circle around to form hollow microspheres.[11] Some self-assembled V_2O_5 bundles of nanorods or nanowires could also be obtained in reverse micelle, after an aging process.[12,13] In this paper, we present a rapid high-yielding facile route to self-assemble V_2O_5 nanowires into bundles with spindle-like morphology by a sonochemical method. This novel synthetic route has some special advantages: straightforward, surfactant/template-free, low-cost, and large-scale production.

In previous studies, 1D V_2O_5 nanoribbon suspensions were easily aligned in rather low AC electric fields and display strong electrooptic effects.[14] The vanadium oxide fibers also show textural anisotropy, as revealed by optical microscopy between crossed polarizers. These outstanding optical properties of 1D nanosized V_2O_5 have encouraged us to develop an optical strategy for sensing biomolecules. The interaction between V_2O_5 and some biomolecules such as protein are of importance, since V_2O_5 is a cause of occupational asthma and chronic bronchitis and increasing evidence indicates that V_2O_5 exerts its effects on cell function by activating the extracellular signal-regulated kinases 1 and 2 (ERK-1/2).[15] 1D highly ordered V_2O_5 nanomaterials as an optical probe for biosensing is highly desirable because of outstanding optical anisotropy and the nonperturbativity of optical sensing. Herein we develop a rapid and sensitive detection method for bovine serum albumin (BSA) based on the self-assembled V_2O_5 bundles via a resonance light scattering technique (RLS). The optical anisotropy of the V_2O_5 bundles−BSA aggregates, as indexed by the Canbennes factor, is also studied by depolarization resonance light scattering (D-RLS).

Experimental Section

Preparation of the V_2O_5 Bundles Samples. In a typical procedure, vanadium oxide (V_2O_5, 0.46 g, 2.5 mmol) and sodium fluoride (NaF, 0.21 g, 5 mmol) were dissolved in 50 mL of distilled water in a 100-mL round-bottom flask. Then the mixture solution was exposed to high-intensity ultrasound irradiation under ambient air for 2 h. Ultrasound irradiation was accomplished with a high-intensity ultrasonic probe (Xinzhi Co., Xinzhi, China; 1.2-cm diameter; Ti-horn, 20 kHz, 100 W/cm^2) immersed directly in the reaction solution. The sonication was conducted without cooling so that the temperature of the reactant

* Author to whom correspondence should be addressed. Fax: +86-25-83594976. E-mail: jjzhu@netra.nju.edu.cn.

10.1021/jp061809m CCC: $33.50
Published on Web 07/11/2006

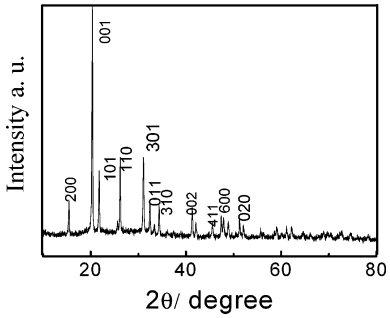

Figure 1. XRD pattern of the V_2O_5 bundles with spindle-like morphology.

mixture increased gradually. When the reaction was finished, a green precipitate was obtained. After cooling of the sample to room temperature, the precipitate was separated by centrifuging at a rotation rate of 9000 rounds/min, washed with distilled water and absolute ethanol in sequence, and dried in air at room temperature.

Characterization Techniques. The products were characterized by XRD (Philip X′pert X-ray diffractometer with Cu Kα radiation, $\lambda = 1.5418$ Å), a transmission electron microscope (TEM; JEOL-JEM 200CX), and a field-emission scanning electron microscope (FE-SEM; LEO-1530VP).

Light scattering studies were performed on a Hitachi 850 Fluorescence spectrophotometer (Tokyo, Japan) at a 90° scattering angle with the passband of the excitation and the emission monochromators at 5.0 nm, using 1-cm quartz cells. The RLS spectra were obtained by synchronously scanning the excitation and emission monochromators in the wavelength region from 300 to 700 nm (namely, $\lambda_{ex} = \lambda_{em}$). The intensity of light scattering was measured at 468 nm where the maximum scattering peak is located. An amount of 1.5 mL of 0.1 M HAc−NaAc buffer (pH = 4.4) was mixed with 1.5 mL of a 40 μg mL^{-1} V_2O_5 bundles solution. Subsequently, an appropriate volume of a solution of 50 μg mL^{-1} bovine serum albumin was added. The mixture was diluted with doubly distilled water to 5.0 mL and mixed thoroughly. The enhancement of light scattering intensity is represented as $\Delta I = I - I_0$, where I and I_0 are the intensity at 468 nm of RLS spectra with and without proteins, respectively. For D-RLS measurements, Glan-Thompson linear polarizers were used to polarize the exciting beam and to analyze the scattered radiation. The scattered light intensities of I_{VH}, I_{VV}, I_{HH}, and I_{HV} were obtained at the wavelength of 468 nm. All measurements were performed at room temperature.

Results and Discussion

Structure and Morphology. The X-ray diffraction (XRD) of the as-prepared self-assembled V_2O_5 bundles is shown in Figure 1. All diffraction peaks can be perfectly indexed to the orthorhombic system with the lattice constants $a = 11.5$, $b = 3.6$, and $c = 4.4$ Å, which are in good agreement with the JCPDS card No. 41-1426. No peaks of any other phases were detected, indicating the high purity of the product.

The size and morphology of the V_2O_5 bundles were examined by FE-SEM (field-emission scanning electron microscope) and TEM (transmission electron microscope). A typical SEM image shown in Figure 2a reveals that the samples are spindle-like morphology with diameters of 400−900 nm at the center and lengths of about 3−7 μm. Furthermore, a high-magnification SEM image (Figure 2b) reveals that the spindle-like V_2O_5 is composed of several tens of homogeneous nanowires with diameters of 30−50 nm and lengths of 3−7 μm. The TEM image in Figure 2c further confirms that the as-prepared V_2O_5 superstructures are indeed the self-assembled V_2O_5 bundles composed of the nanowires. The EDX analysis in Figure 2d shows that the chemical signature of the nanowires is identical within experimental error and that these nanowires are composed of V and O elements with a ratio of O/V being about 2.2:1. The other peak originates from the substrate of the sample disk.

Possible Formation Mechanism. In the reaction system, the alkali salts (e.g., NaF, NaCl, $NaNO_3$, Na_2SO_4, KCl, KNO_3, or K_2SO_4) were used as mineralizers. It was observed that mineralizers had a great influence on the morphologies of the synthesized vanadium precursors. Without the mineralizer in the reaction, the nanowire cannot be obtained, just some larger particles were observed. Therefore, the presence of the mineralizer is an important factor for influencing the growth of the V_2O_5 nanostructures. On one hand, these mineralizers can increase the chemical potential of the solution, and higher chemical potential conditions would be advantageous for 1D

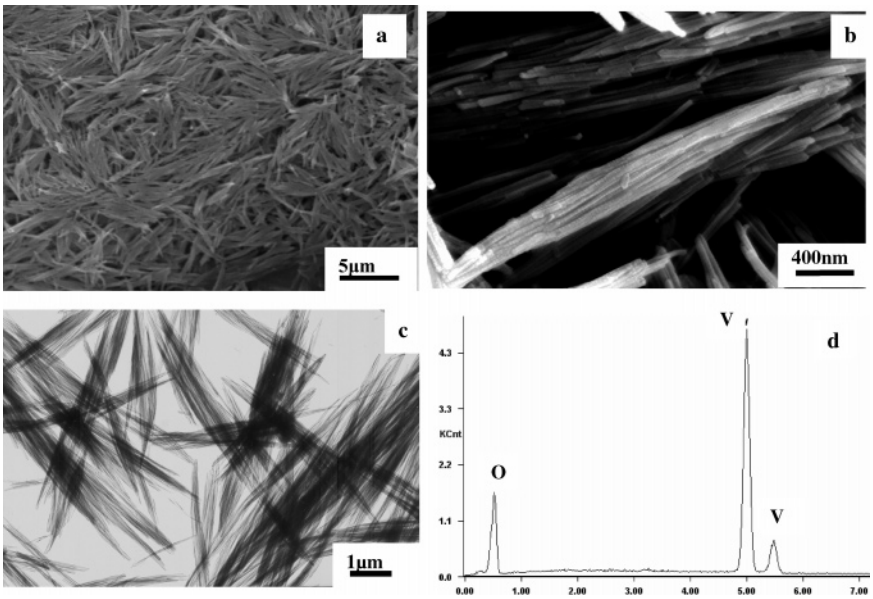

Figure 2. FE-SEM images of the V_2O_5 bundles with spindle-like morphology: (a) low-magnification SEM image of V_2O_5 bundles; (b) high-magnification SEM image, (c) low-magnification TEM image; (d) energy-dispersive X-ray image.

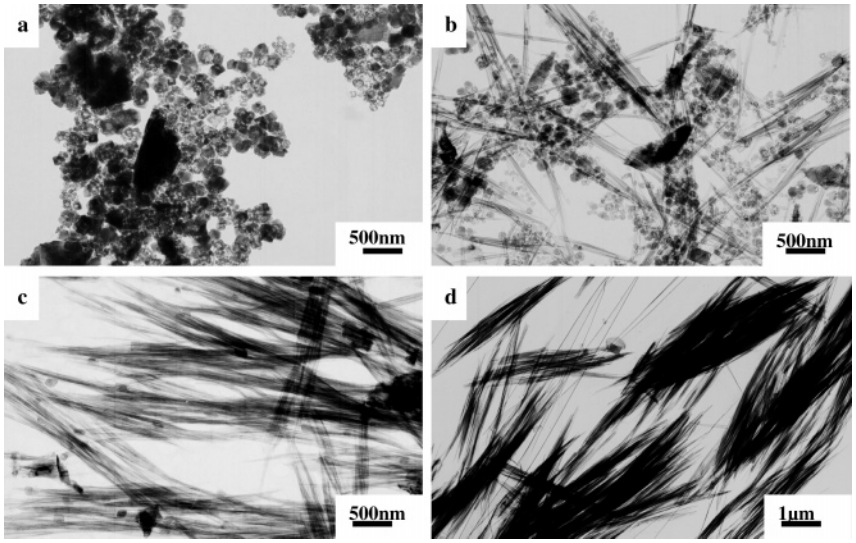

Figure 3. TEM images of the sample collected at different stages: (a) 0.5 h, (b) 1 h, (c) 1.5 h, and (d) 2 h.

SCHEME 1: Schematic Illustration of the Growth Mechanism of the V_2O_5 Bundles

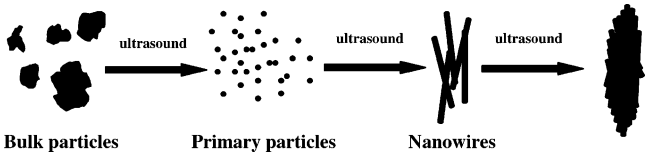

nanostructure growth. Meanwhile, the addition of mineralizers can increases the mobility of the components in the system and allows atoms, ions, or molecules to adopt appropriate positions in developing crystal lattices. Thus, the addition of salts can provide a favorable environment for the growth of nanowires.[16−18]

Time-dependent experiments were performed to gain an insight into the formation process of the sample. The self-assembled V_2O_5 bundles with spindle-like morphology were characterized by TEM at various stages of the growth process. Figure 3 shows the images taken from the reaction mixture after the solution was exposed to high-intensity ultrasound irradiation under ambient conditions for 0.5, 1, 1.5, and 2 h. In Figure 3a, it was obvious that the large V_2O_5 particles were observed in the initial reaction mixture. As the reaction time increased, the amounts of initial particles decreased. When the reaction time reached 1 h, the particles began to grow up and the wires were observed (Figure 3b). Therefore, these small particles would serve as seeds for the growth of V_2O_5 nanowires. When the reaction time reached 1.5 h, the V_2O_5 nanowires were the main morphology (Figure 3c). After 2 h, the reaction was finished, and the V_2O_5 nanowires reached a stable state (Figure 3d).

The formation of V_2O_5 nanowires and then their self-assembly could be related to one proposed mechanism, so-called "self-assembly and oriented attachment" by Qi.[19] There are some similarities in our system with their studies. Therefore, we believe that the sonochemical formation of self-assembled V_2O_5 bundles underwent three steps in sequence: (1) ultrasound-induced dissolution of V_2O_5 and formation of nuclei, which led to primary nanoparticles; (2) ultrasound-induced fusion of these primary nanoparticles accompanying oriented attachment to form the nanowires; and (3) the individual nanowires were further attached side-by-side to assemble into bundles, accompanying an Ostwald ripening process. A schematic illustration of the development of self-assembled V_2O_5 bundles is shown in Scheme 1.

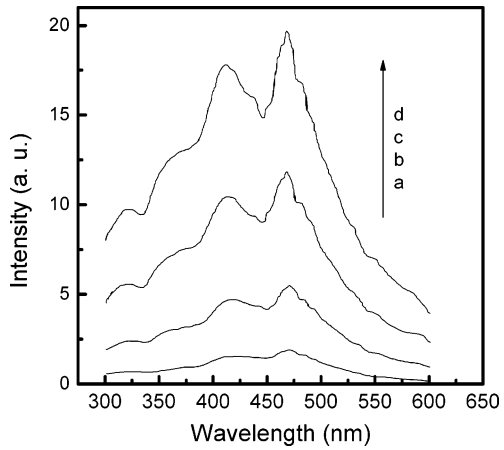

Figure 4. Resonance light scattering spectra of a BSA−V_2O_5 bundles system at pH = 4.4; BSA (μg mL^{-1}): a, 0; b, 4; c, 10; and d, 16.

Resonance Light Scattering Sensing for Bovine Serum Albumin. In our study, a resonance light scattering technique was employed to detect bovine serum albumin on the basis of the self-assembled V_2O_5 bundles. Figure 4 shows the RLS spectra of the V_2O_5 and the mixtures of V_2O_5 with various BSA concentrations. Both the RLS spectra of V_2O_5 bundles in the absence and presence of BSA have similar features and presented two peaks at 410 and 468 nm.

The scattered light signals of V_2O_5 bundles were enhanced by the addition of BSA. We selected the maximum wavelength at 468 nm for the detection of BSA with high sensitivity. It was found that the enhanced RLS intensity at 468 nm of V_2O_5 bundles−BSA varies linearly with the concentration of BSA in the range from 0.5 to 20 μg mL^{-1} (Figure 5). The linear regression equation is $\Delta I = 1.196c - 1.09$, with a correlation coefficient of $R = 0.998$ and a detection limit (3σ) of 0.13 μg mL^{-1}. As reported in the literature, BSA has a rather weak RLS signal.[20] In our experiments, the RLS intensities of BSA in a NaAc−HAc buffer solution (pH 4.4) are less than 0.5% that of V_2O_5 bundles−BSA, even if the BSA concentration is up to 20 μg mL^{-1}. Thus, the scattered light from BSA can be neglected. According to the RLS theory, the increase in the scatterer volume results in the enhanced light scattering signals.[21−24] Thus we attribute the enhanced RLS intensities to the aggregation behavior between V_2O_5 bundles and BSA.

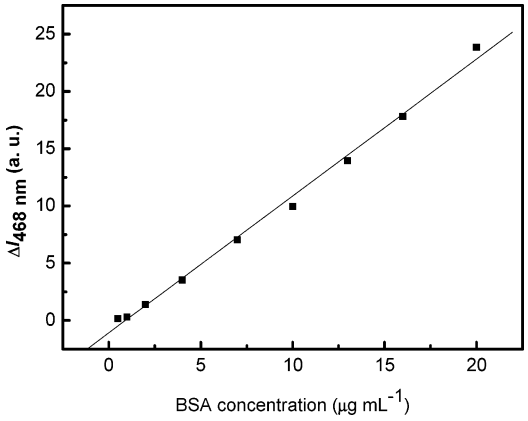

Figure 5. Calibration curve for the detection of BSA. The curves represent a linear fit to the data points.

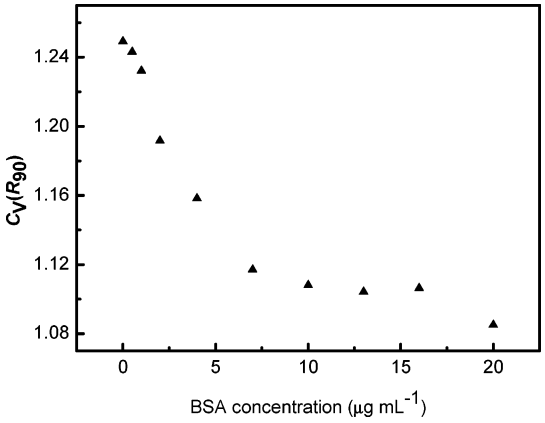

Figure 6. Dependence of the Cabannes factor of BSA−V_2O_5 bundles aggregates on BSA concentration.

As light is scattered from an anisotropic particle, or particle aggregates, the depolarization ratio of scattered light is defined as[25−27]

$$\rho_V = \frac{I_{VH}}{I_{VV}} \tag{1}$$

where subscript V refers to the fact that the incident light is vertically polarized, and I_{VH} and I_{VV} are the intensities of the horizontally and vertically polarized components of the scattered light, respectively. It is necessary to correct the value of I_{VH} for the polarization-dependent response of the emission monochromator. Hence, the measured quantity is[28]

$$\rho_{V,Corr} = G\rho_V \tag{2}$$

where $G = I_{HV}/I_{HH}$ is the correction factor, and I_{HV} and I_{HH} are the intensities of the vertically and horizontally polarized components of the scattered light when the incident light is horizontally polarized. A term known as the Cabannes factor is used to correct the Rayleigh ratio for deviations due to anisotropy. At an observation angle θ of 90°, the Cabannes factor is defined as[26,27]

$$C_V(R_{90}) = \left(\frac{3 + 3\rho_{V,Corr}}{3 - 4\rho_{V,Corr}}\right) \tag{3}$$

As a correction term of the Rayleigh ratio for a system of anisotropic particles, the Cabannes factor appears to be a convenient index with which to study the optical anisotropy of macromolecules. Striegel developed a depolarization multi-angle light scattering method to determine the Cabannes factor of polymers, as a continuous function of molar mass and at discrete angular intervals.[26] Here, we investigated the interaction between V_2O_5 bundles and BSA by using depolarization resonance light scattering (D-RLS). To our knowledge, this is first observation of the dependence of the Cabannes factor on BSA concentration.

Results of the D-RLS experiments are shown in Figure 6. The Cabannes factor is calculated from the light scattering data by eq 3. Due to the anisotropic morphology, a large Cabannes factor value ($C_V(R_{90}) = 1.249$) was expected for the V_2O_5 bundles. After the V_2O_5 bundles−BSA aggregates are formed through electrostatic force and hydrogen bonds, the Cabannes factor is significantly decreased with increased BSA concentration up to about 7 μg mL^{-1}. Then, the Cabannes factor gently decreases toward high BSA concentrations ranging from 10 to 20 μg mL^{-1}. The decreased rigidity of the V_2O_5 bundles−BSA aggregates with increasing flexible BSA molecules is seen to result in decreased depolarization of the scattered light. In a previous study of the depolarization behavior of brominated polystyrene (PSBr),[27] the corresponding increases in the Cabannes factors are evident at all angles with decreasing molar mass. Moreover, the distribution of the Cabannes factor is a continuous function of molar mass. Interestingly, our findings that the Cabannes factor of V_2O_5 bundles−BSA aggregates decreases as the BSA concentration increases closely resemble results reported in the depolarization behavior of the PSBr macromolecule.[28]

We propose that the V_2O_5 bundles−BSA aggregate behaves as a supramolecule consisting of V_2O_5 bundles and BSA molecules. The molar mass of the V_2O_5 bundles−BSA aggregate could be expressed as

$$M_{aggregate} = \frac{n_{V_2O_5bundles}M_{V_2O_5bundles} + n_{BSA}M_{BSA}}{n_{V_2O_5bundles} + n_{BSA}} \tag{4}$$

where $n_{V_2O_5bundles}$ and n_{BSA} are the number of moles of V_2O_5 bundles and BSA in the aggregates, and $M_{V_2O_5bundles}$ and M_{BSA} are the molar mass of V_2O_5 bundles and BSA, respectively. It is clear that as BSA concentration of the aggregate increases, $M_{aggregate}$ increases. Thus, we may conclude that the Cabannes factor for the V_2O_5 bundles−BSA aggregates is seen to be molar-mass-dependent, resembling the results reported in the Cabannes factor for the anisotropic PSBr polymer.[28]

Conclusion

In summary, a rapid high-yielding method has been developed to synthesize self-assembled V_2O_5 with highly ordered superstructures in which nanowires interconnect to form the V_2O_5 bundles with spindle-like morphology. The formation mechanism of the spindle-like structure has also been investigated. We also develop a sensitive resonance light scattering method for the detection of BSA on the basis of self-assembled V_2O_5 bundles. The results of the polarized resonance light scattering demonstrated that the Cabannes factor for the V_2O_5 bundles−BSA aggregates is BSA concentration-dependent.

Acknowledgment. This work was supported by the National Natural Science Foundation of China (No. 20325516, 90206037, 20521503) and Jiangsu Scientific Project (BK2004210).

References and Notes

(1) Biette, L.; Carn, F.; Maugey, M.; Achard, M.-F.; Maquet, J.; Steunou, N.; Livage, J.; Serier, H.; Backov, R. *Adv. Mater.* **2005**, *17*, 2970.

(2) Yu, H. Y.; Kang, B. H.; Pi, U. H.; Park, C. W.; Choi, S. Y. *Appl. Phys. Lett.* **2005**, *86*, 253102.
(3) Liu, J. F.; Wang, X.; Peng, Q.; Li, Y. D. *Adv. Mater.* **2005**, *17*, 764.
(4) Micocci, G.; Serra, A.; Tepore, A.; Capone, S. *J. Vac. Sci. Technol. A* **1997**, *15*, 34.
(5) Niederberger, M.; Muhr, H. J.; Krumeich, F.; Bieri, F.; Günther, D.; Nesper, R. *Chem. Mater.* **2000**, *12*, 1995.
(6) Spahr, M. E.; Bitterli, P.; Nesper, R.; Müller, M.; Krumeich, F.; Nissen, H. U. *Angew. Chem., Int. Ed. Engl.* **1998**, *37*, 1263.
(7) Muhr, H. J.; Krumeich, F.; Schönholzer, U. P.; Bieri, F.; Niederberger, M.; Gauckler, L. J.; Nesper, R. *Adv. Mater.* **2000**, *12*, 231.
(8) Muster, J.; Kim, G. T.; Krsticæ, V.; Park, J. G.; Park, Y. W.; Roth, S.; Burghard, M. *Adv. Mater.* **2000**, *12*, 420.
(9) Gu, Z.; Fan, R.; Mo, W.; Chen, X.; Yang, L.; Zhang, S.; Hu, Y.; Wang, Z.; Fan, W. *Chem. Mater.* **2002**, *14*, 5053.
(10) Chandrappa, G. T.; Steunou, N.; Cassaignon, S.; Bauvais, C.; Livage, J. *Catal. Today* **2003**, *78*, 85
(11) Cao, A. M.; Hu, J. S.; Liang, H. P.; Wan, L. J. *Angew. Chem., Int. Ed.* **2005**, *44*, 4391.
(12) Pinna, N.; Willinger, M.; Weiss, K.; Urban, J.; Schlögl, R. *Nano Lett.* **2003**, *3*, 1131.
(13) Pinna, N.; Wild, U.; Urban, J.; Schlögl, R. *Adv. Mater.* **2003**, *15*, 329.
(14) Lamarque-Forget, S.; Pelletier, O.; Dozov, I.; Davidson, P.; Martinot-Lagarde, P.; Livage, J. *Adv. Mater.* **2000**, *12*, 1267.
(15) Wang, Y. Z.; Bonner, J. C. *Am. J. Respir. Cell Mol. Biol.* **2000**, *22*, 590.
(16) Trentler, J. W.; Hickman, S. C.; Viano, A. M.; Gibbons, P. C.; Buhro, W. E. *Science* **1995**, *270*, 1791.
(17) Peng, Z. A.; Peng, X. *J. Am. Chem. Soc.* **2001**, *123*, 1389.
(18) Wang, X.; Li, Y. D. *Angew. Chem., Int. Ed.* **2002**, *41*, 4790.
(19) Lu, C. H.; Qi, L. M.; Yang, J. H.; Zhang, D. Y.; Wu, N. Z.; Ma, J. M. *J. Phys. Chem. B* **2004**, *108*, 17825.
(20) Li, Y. F.; Huang, C. Z.; Huang, X. H.; Li, M. *Anal. Sci.* **2000**, *16*, 1249.
(21) Pasternack, R. F.; Bustamante, C.; Collings, P. J.; Giannetto, A.; Gibbs, E. J. *J. Am. Chem. Soc.* **1993**, *115*, 5393.
(22) Pasternack, R. F.; Collings, P. J. *Science* **1995**, *269*, 935.
(23) Huang, C. Z.; Li, Y. F. *Anal. Chim. Acta* **2003**, *500*, 105.
(24) Yguerabide, J.; Yguerabide, E. E. *Anal. Biochem.* **1998**, *262*, 137.
(25) Kokhanovsky, A. A.; Jones, A. R. *J. Phys. D: Appl. Phys.* **2002**, *35*, 1903.
(26) Striegel, A. M. *Anal. Chem.* **2002**, *74*, 3013.
(27) Striegel, A. M. *Polym. Int.* **2003**, *52*, 1863.
(28) Parkash, J.; Robblee, J. H.; Agnew, J.; Gibbs, E.; Collings, P.; Pasternack, R. F.; de Paula, J. C. *Biophys. J.* **1998**, *74*, 2089.